LAMB WAVE SCATTERING FROM RIVETS

Mark K. Hinders
Department of Applied Science
The College of William & Mary
Williamsburg, VA 23187-8795

INTRODUCTION

For structures with large surface areas, a full integrity evaluation can be a time-consuming operation. Lamb wave techniques allow this evaluation to be performed with waves propagating along one dimension of the inspection area while the probing transducers are moved in the perpendicular dimension, giving information about the presence of flaws within the entire scanned area. For riveted structures the scattering of the Lamb waves from the rivets is often the dominant feature in the measured response, masking the more subtle effects of Lamb wave interactions with the flaws of interest [1]. In this paper we consider the scattering of lowest mode symmetric and antisymmetric Lamb waves from model rivets, and derive analytic expressions for the scattered fields. With solutions of this type the disruptive effects of the rivets can be "processed out" of measured data in order to expose the signals which are due to the flaws in the structure.

The paper is organized as follows. We first discuss flexural wave scattering from in-plane disks in order to model lowest-order antisymmetric Lamb wave (A0) scattering from rivets. Next we similarly discuss extensional wave scattering from disks in order to model lowest-order symmetric Lamb wave (S0) scattering from rivets. In both cases exact and analytic eigenfunction solutions to the scattering problems are derived, and these solutions are implemented to plot the angular distribution of the scattered Lamb waves. For the A0 Lamb wave modes we use the classical theory of flexural plate motions [2], but for the S0 modes the elementary Poisson theory for the stretching of a plate of uniform thickness cannot describe dispersion. Instead, we use the method of Mindlin et al. [3] – [6] which takes into account the coupling between extensional symmetric thickness-stretch and thickness-shear modes. We have not found it necessary to use Mindlin's corresponding theory for flexural motions [7], [8] because the simple plate theory accounts for dispersion. Finally, we discuss the results and some implications for the nondestructive evaluation of aging aircraft structures with portable ultrasonic Lamb wave scanning devices.

FLEXURAL WAVE SCATTERING FROM IN-PLANE DISKS

The displacement of a plate in bending is given by the well-known plate equation

$$D\nabla^2\nabla^2 w + 2h\rho\partial_t^2 w = q \tag{1}$$

where w is the transverse displacement of the plate. Here $2h$ is the thickness of the plate, ρ is its density and D is given by

$$D = \frac{2\mu I}{1-\nu} = \frac{2Eb^3}{3(1-\mu^2)} \qquad I = 2h^3/3$$

Review of Progress in Quantitative Nondestructive Evaluation, Vol. 15
Edited by D.O. Thompson and D.E. Chimenti, Plenum Press, New York, 1996

where E, ν, μ are Young's modulus, Poisson's ratio, and rigidity of the material. The in-plane disk scatterer of radius $r = a$ is located at the origin of the coordinate system. A prime will be used to indicate its material parameters, which are different from those of the surrounding plate. For $q = 0$ and harmonic wave motion solutions to the equation of motion are

$$w(x, y, t) = [W_p(x, y) + W_a(x, y)]\, e^{-i\omega t} \tag{2}$$

where $W_{p,a}$ satisfy

$$(\nabla^2 + \gamma^2)W_p = 0 \qquad\qquad (\nabla^2 - \gamma^2)W_a = 0 \tag{3}$$

with $\gamma = \omega\sqrt{2h\rho/D}$. Note that W_p represents the part of the flexural wave that travels with the speed $c_f = \gamma\sqrt{D/2h\rho}$ and W_a represents the part attenuating as it progresses.

If the disk scatterer (rivet) is at a large distance from the source the attenuation will reduce W_a to a negligible amount and only W_p needs to be considered as the incident plane flexural wave. We write it as

$$w^{inc} = w_0 e^{i(\gamma x - \omega t)} = w_0 \sum_{n=0}^{\infty} \epsilon_n i^n J_n(\gamma r) \cos n\theta e^{-i\omega t} \tag{4}$$

In polar coordinates the solutions for $W_{p,a}$ are of the form $H_n(\gamma r)e^{\pm in\theta}$ and $H_n(i\gamma r)e^{\pm in\theta}$ respectively so we can write the scattered flexural wave as

$$w^{scat} = w_0 \sum_{n=0}^{\infty} \epsilon_n i^n \left[A_n H_n(\gamma r) + B_n H_n(i\gamma r)\right] \cos n\theta e^{-i\omega t} \tag{5}$$

Inside the rivet the refracted waves are standing waves which can be represented as

$$w^{refr} = w_0 \sum_{n=0}^{\infty} \epsilon_n i^n \left[C_n J_n(\gamma' r) + D_n J_n(i\gamma' r)\right] \cos n\theta e^{-i\omega t} \tag{6}$$

In these $J_n(\cdot)$ and $H_n(\cdot)$ are the usual Bessel and Hankel functions, and ϵ_n is 1 for $n = 0$ and 2 otherwise. In polar coordinates the boundary conditions at $r = a$ are continuity of transverse displacements and shear forces as well as slope and bending moment. The needed bending moments and transverse shear forces are given by

$$M_{rr} = -D\left[\nu\nabla^2 w + (1 - \nu)\partial_r^2 w\right]$$

and

$$V_r = -D\partial_r(\nabla^2 w) - \frac{1}{r}\partial_\theta\left\{D(1 - \nu)\partial_r\left(\frac{1}{r}\partial_\theta w\right)\right\}$$

For a rivet the following four conditions must be satisfied at the boundary $r = a$:

$$w^{inc} + w^{scat} = w^{refr} \qquad\qquad \partial_r w^{inc} + \partial_r w^{scat} = \partial_r w^{refr} \tag{7}$$

$$M_{rr}^{inc} + M_{rr}^{scat} = M_{rr}^{refr} \qquad\qquad V_r^{inc} + V_r^{scat} = V_r^{refr}$$

These give rise to four simultaneous equations for the unknown coefficients A_n, B_n, C_n, D_n. Solving this system algebraically gives for $A_n = -\frac{J_n(\gamma a)}{H_n(\gamma a)}\frac{\Delta_1}{\Delta_0}$:

$$\begin{aligned}\Delta_0 \;=\; & \left(\frac{\gamma' a J_n'(\gamma' a)}{J_n(\gamma' a)} + \frac{i\gamma' a J_n'(i\gamma' a)}{J_n(i\gamma' a)}\right)\left(\frac{\gamma a H_n'(\gamma a)}{H_n(\gamma a)} + \frac{i\gamma a H_n'(i\gamma a)}{H_n(i\gamma a)}\right)\left\{-2 + \right. \\ & \left(\frac{\frac{\gamma a H_n'(\gamma a)}{H_n(\gamma a)} - \frac{i\gamma a H_n'(i\gamma a)}{H_n(i\gamma a)}}{\frac{\gamma a H_n'(\gamma a)}{H_n(\gamma a)} + \frac{i\gamma a H_n'(i\gamma a)}{H_n(i\gamma a)}}\right)\left(\frac{i\gamma' a J_n'(i\gamma' a)}{J_n(i\gamma' a)} - n^2\frac{p-1}{x'^2}\right)\frac{p-1}{x^2} + \left(\frac{\frac{\gamma' a J_n'(\gamma' a)}{J_n(\gamma' a)} - \frac{i\gamma' a J_n'(i\gamma' a)}{J_n(i\gamma' a)}}{\frac{\gamma' a J_n'(\gamma' a)}{J_n(\gamma' a)} + \frac{i\gamma' a J_n'(i\gamma' a)}{J_n(i\gamma' a)}}\right)\frac{i\gamma a H_n'(i\gamma a)}{H_n(i\gamma a)}\frac{p-1}{x'^2}\Bigg\} \\ & + \left(\frac{x}{x'}\right)^2\left(\frac{\gamma a H_n'(\gamma a)}{H_n(\gamma a)} - \frac{i\gamma a H_n'(i\gamma a)}{H_n(i\gamma a)}\right)\left\{2n^2\frac{p-1}{x'^2}\left[1 + \frac{i\gamma' a J_n'(i\gamma' a)}{J_n(i\gamma' a)}\frac{p-1}{x'^2}\right]\right. \\ & \left. + \left(\frac{\gamma' a J_n'(\gamma' a)}{J_n(\gamma' a)} - \frac{i\gamma' a J_n'(i\gamma' a)}{J_n(i\gamma' a)}\right)\left[2 + \frac{i\gamma a H_n'(i\gamma a)}{H_n(i\gamma a)}\frac{p-1}{x^2} + \frac{i\gamma' a J_n'(i\gamma' a)}{J_n(i\gamma' a)}\frac{p-1}{x'^2}\right]\right\}\end{aligned} \tag{8}$$

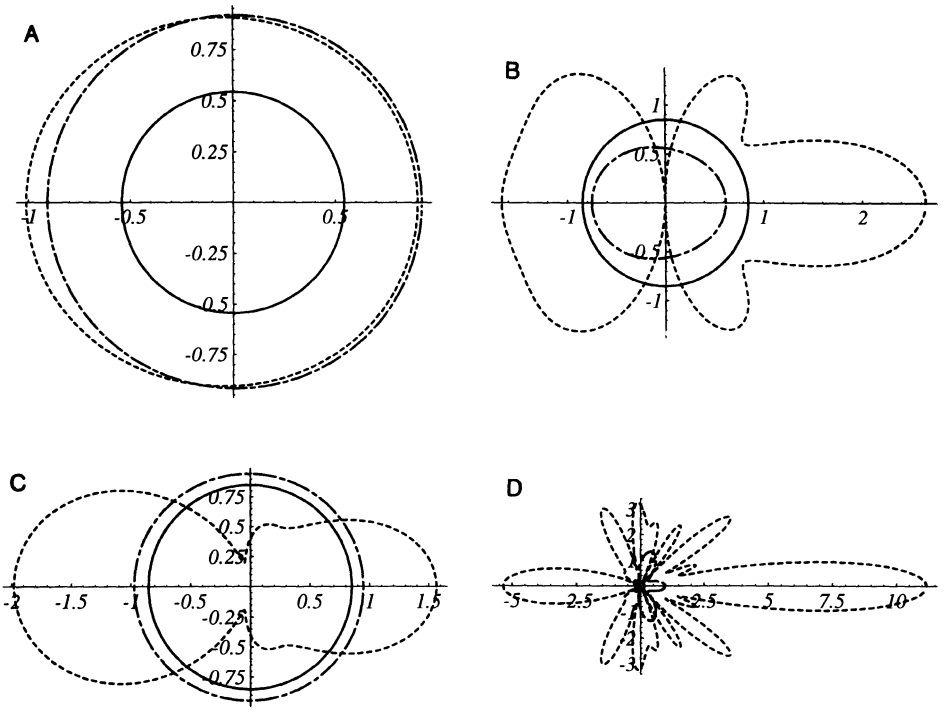

Figure 1: Angular far-field scattering for in-plane steel disk in aluminum plate. In each the solid line is for $\omega/\omega_0 = 0.1$, the long-short dashed line is for $\omega/\omega_0 = 0.5$, and the dashed line is for $\omega/\omega_0 = 0.9$. The four plots are for (A) $a/h = 0.1$, (B) $a/h = 0.5$, (C) $a/h = 1.0$, (D) $a/h = 10$.

$$\Delta_1 = \left(\frac{\gamma' a J_n'(\gamma' a)}{J_n(\gamma' a)} + \frac{i\gamma' a J_n'(i\gamma' a)}{J_n(i\gamma' a)}\right)\left(\frac{\gamma a J_n'(\gamma a)}{J_n(\gamma a)} + \frac{i\gamma a H_n'(i\gamma a)}{H_n(i\gamma a)}\right)\{-2+ \tag{9}$$

$$\left(\frac{\frac{\gamma a J_n'(\gamma a)}{J_n(\gamma a)} - \frac{i\gamma a H_n'(i\gamma a)}{H_n(i\gamma a)}}{\frac{\gamma a J_n'(\gamma a)}{J_n(\gamma a)} + \frac{i\gamma a H_n'(i\gamma a)}{J_n(i\gamma a)}}\right)\left(\frac{i\gamma' a J_n'(i\gamma' a)}{J_n(i\gamma' a)} - n^2\frac{p-1}{x'^2}\right)\frac{p-1}{x^2} + \left(\frac{\frac{\gamma' a J_n'(\gamma' a)}{J_n(\gamma' a)} - \frac{i\gamma' a J_n'(i\gamma' a)}{J_n(i\gamma' a)}}{\frac{\gamma' a J_n'(\gamma' a)}{J_n(\gamma' a)} + \frac{i\gamma' a J_n'(i\gamma' a)}{J_n(i\gamma' a)}}\right)\frac{i\gamma a H_n'(i\gamma a)}{H_n(i\gamma a)}\frac{p-1}{x'^2}\Bigg\}$$

$$+\left(\frac{x}{x'}\right)^2\left(\frac{\gamma a J_n'(\gamma a)}{J_n(\gamma a)} - \frac{i\gamma a H_n'(i\gamma a)}{H_n(i\gamma a)}\right)\left\{2n^2\frac{p-1}{x'^2}\left[1 + \frac{i\gamma' a J_n'(i\gamma' a)}{J_n(i\gamma' a)}\frac{p-1}{x'^2}\right]\right.$$

$$\left.+\left(\frac{\gamma' a J_n'(\gamma' a)}{J_n(\gamma' a)} - \frac{i\gamma' a J_n'(i\gamma' a)}{J_n(i\gamma' a)}\right)\left[2 + \frac{i\gamma a H_n'(i\gamma a)}{H_n(i\gamma a)}\frac{p-1}{x^2} + \frac{i\gamma' a J_n'(i\gamma' a)}{J_n(i\gamma' a)}\frac{p-1}{x'^2}\right]\right\}$$

where we have defined $p = D'/D$ and $x^2 = (\gamma a)^2/(\nu - 1)$. Similar expressions can be derived for B_n, C_n, D_n in order to specify analytically the scattered and refracted fields that result from interaction of the incident flexural wave with the rivet.

In the far-field of the rivet the scattered field will consist of only the propagating part, so B_n is not needed, and we can exploit the large argument properties of the Hankel functions to write

$$w^{scatt} \to \sqrt{\frac{2}{i\pi\gamma r}}e^{i(\gamma r)}w_0 e^{-i\omega t}\sum_{n=0}^{\infty}\epsilon_n A_n \cos n\theta \tag{10}$$

Figures 1 and 2 show the angular distribution of the $A0$ scattering amplitude for in-plane steel and titanium disks in an aluminum plate. The four plots in each are for different values of the ratio of disk radius to plate semithickness, and for each plot three curves are superimposed for three different frequencies. The plane wave is incident from the left, with the rivet at the origin of the coordinate system.

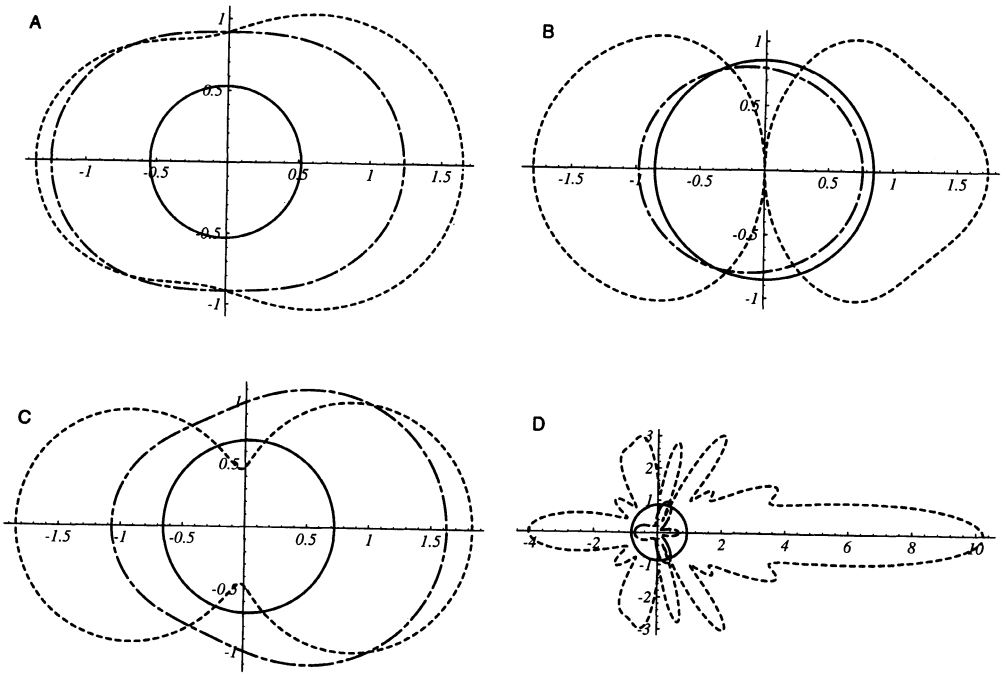

Figure 2: Angular far-field scattering for in-plane titanium disk in aluminum plate. In each the solid line is for $\omega/\omega_0 = 0.1$, the long-short dashed line is for $\omega/\omega_0 = 0.5$, and the dashed line is for $\omega/\omega_0 = 0.9$. The four plots are for (A) $a/h = 0.1$, (B) $a/h = 0.5$, (C) $a/h = 1.0$, (D) $a/h = 10$.

DILATATIONAL WAVE SCATTERING FROM IN-PLANE DISKS

In order to model the scattering of the lowest-order symmetric Lamb wave modes from rivets it is necessary to go to a slightly more complicated theory than was used for the anti-symmetric modes. This is because the simplest plate theories give only that portion of the $S0$ curve which is dispersionless. Since we are interested in modelling measurements made on the shoulder of that curve, we need to account for the dispersive effects. Without resorting to a full three-dimensional elasticity treatment, Kane and Mindlin [3] – [6] provide us with an appropriate theory for dilatational plate wave scattering from rivets.

As in the previous section we consider an infinite plate that is homogeneous, isotropic and linearly elastic. We assume that the plate is bounded by the planes $z = \pm h$ and that there is an in-plane disk of radius $r = a$ at the origin of a cylindrical coordinate system. The model rivet (disk) is a similar material, but with arbitrarily different material parameters. We describe the plate by density ρ and Lame parameters λ, μ. The rivet is described by ρ' and λ', μ'. The wave speeds for bulk longitudinal and transverse waves as well as the limiting value for plate waves are given by

$$c_L = \sqrt{\frac{\lambda + 2\mu}{\rho}} \qquad c_T = \sqrt{\frac{\mu}{\rho}} \qquad c_P = \sqrt{\frac{4\mu(\lambda+\mu)}{\rho(\lambda+2\mu)}}$$

For thin plates we assume that the components of displacement in cylindrical coordinates are approximated sufficiently well by

$$u_r(r,\theta,t) = v_r(r,\theta,t) \qquad u_\theta(r,\theta,t) = v_\theta(r,\theta,t) \qquad u_z(r,\theta,t) = \frac{z}{h} v_z(r,\theta,t) \tag{11}$$

and that the strain-displacement equations are

$$\sigma_{rr} = (\lambda + 2\mu)\epsilon_{rr} + \lambda(\epsilon_{\theta\theta} + \kappa\epsilon_{zz})$$

$$\begin{aligned} \sigma_{\theta\theta} &= (\lambda+2\mu)\epsilon_{\theta\theta} + \lambda(\epsilon_{rr}+\kappa\epsilon_{zz}) \\ \sigma_{zz} &= (\lambda+2\mu)\kappa^2\epsilon_{zz} + \lambda\kappa(\epsilon_{rr}+\epsilon_{\theta\theta}) \end{aligned} \qquad (12)$$

$$\sigma_{r\theta} = \mu\epsilon_{r\theta} \qquad \sigma_{rz} = \mu\epsilon_{rz} \qquad \sigma_{\theta z} = \mu\epsilon_{\theta z}$$

Note the constant $\kappa = \pi/\sqrt{12}$ which has been inserted to improve the results. We then introduce three independent displacement potentials $\phi_1(r,\theta), \phi_2(r,\theta), \psi(r,\theta)$ defined by

$$\begin{aligned} v_r &= \left(\frac{\partial\phi_1}{\partial r} + \frac{\partial\phi_2}{\partial r} + \frac{1}{r}\frac{\partial\psi}{\partial\theta}\right) e^{-i\omega t} \\ v_\theta &= \left(\frac{1}{r}\frac{\partial\phi_1}{\partial\theta} + \frac{1}{r}\frac{\partial\phi_2}{\partial\theta} - \frac{\partial\psi}{\partial r}\right) e^{-i\omega t} \\ v_z &= \left(\frac{\sigma_1}{h}\phi_1 + \frac{\sigma_2}{h}\phi_2\right) e^{-i\omega t} \end{aligned} \qquad (13)$$

so that the displacement potentials each satisfy a scalar Helmholtz equation:

$$\left(\nabla^2 + k_1^2\right)\phi_1 = 0 \qquad \left(\nabla^2 + k_2^2\right)\phi_1 = 0 \qquad \left(\nabla^2 + K^2\right)\psi_1 = 0 \qquad (14)$$

In these equations we have used the terms

$$\sigma_{1,2} = \frac{\lambda+\mu}{\pi\lambda/\sqrt{12}}\left(k_{1,2}^2 - \frac{\omega^2}{c_L^2}\right) \qquad K^2 = \frac{\omega^2}{c_T^2}$$

$$k_{1,2}^2 = \frac{3}{2}\left(\frac{\pi^2}{12h}\right)^2 \left\{ \left(\frac{c_L^2}{c_T^2}+1\right)\frac{\omega^2}{\omega_0^2} - \frac{c_P^2}{c_T^2} \pm \sqrt{\left[\left(\frac{c_L^2}{c_T^2}+1\right)\frac{\omega^2}{\omega_0^2} - \frac{c_P^2}{c_T^2}\right]^2 + 4\frac{c_L^2}{c_T^2}\frac{\omega^2}{\omega_0^2}\left(1-\frac{\omega^2}{\omega_0^2}\right)} \right\}$$

where $\omega_0^2 = \pi\sqrt{c_L}/4h^2$. The stress components needed along with (13) for the welded-contact boundary conditions are then given by, suppressing $e^{-i\omega t}$ time variation,

$$\begin{aligned} \sigma_{rr} &= (\lambda+2\mu)\frac{\partial v_r}{\partial r} + \lambda\left(\frac{1}{r}\frac{\partial v_\theta}{\partial\theta} + \frac{v_r}{r} + \frac{v_z}{h}\right) \\ \sigma_{r\theta} &= \mu\left(\frac{1}{r}\frac{\partial v_r}{\partial\theta} + \frac{\partial v_\theta}{\partial r} - \frac{v_\theta}{r}\right) \qquad \sigma_{rz} = \mu\left(\frac{z}{h}\frac{\partial v_z}{\partial r}\right) \end{aligned} \qquad (15)$$

Now consider an incident plane wave described by

$$\phi_1^{inc} = e^{ik_1 x} \qquad \phi_2^{inc} = \psi^{inc} = 0 \qquad (16)$$

and expand scattered and transmitted waves in terms of the general solutions of the scalar wave equation:

$$\begin{aligned} \phi_1^{scat} &= \sum_{n=-\infty}^{\infty} A_n i^n H_n(k_1 r) e^{in\theta} \\ \phi_2^{scat} &= \sum_{n=-\infty}^{\infty} B_n i^n H_n(k_2 r) e^{in\theta} \\ \psi^{scat} &= \sum_{n=-\infty}^{\infty} C_n i^n H_n(K r) e^{in\theta} \\ \phi_1^{trans} &= \sum_{n=-\infty}^{\infty} A_n' i^n J_n(k_1' r) e^{in\theta} \\ \phi_2^{trans} &= \sum_{n=-\infty}^{\infty} B_n' i^n J_n(k_2' r) e^{in\theta} \\ \psi^{trans} &= \sum_{n=-\infty}^{\infty} C_n' i^n J_n(K' r) e^{in\theta} \end{aligned} \qquad (17)$$

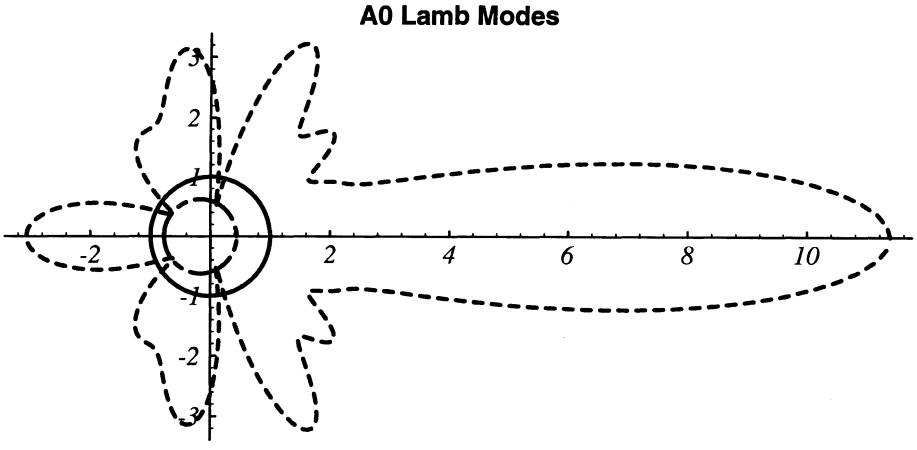

Figure 3: Angular scattering of S0-Lamb waves from in-plane steel disk in aluminum plate. The solid line is for $\gamma a = 0.1$, the long-short dashed line is for $\gamma a = 1.0$, and the dashed line is for $\gamma a = 10$.

where $A_n, \ldots, C'_n$ are unknown modal coefficients to be determined from the boundary conditions. Note that the incident plane wave potential can also be expanded in cylindrical functions:

$$\phi_1^{inc} = e^{ik_1 r\cos\theta} = \sum_{n=-\infty}^{\infty} i^n J_n(k_1 r) e^{in\theta} \tag{18}$$

Applying boundary conditions we find the coefficients to be $A_n = \frac{\Delta_1}{\Delta_0}$ and $B_n = \frac{\Delta_2}{\Delta_0}$ where

$$\begin{aligned}\Delta_0 &= \left(\frac{k'_1 a J'_n(k'_1 a)}{J_n(k'_1 a)} - \frac{k'_2 a J'_n(k'_2 a)}{J_n(k'_2 a)}\right)\left[\left(\frac{k_2 a H'_n(k_2 a)}{H_n(k_2 a)} - 1\right)\beta_1 - \left(\frac{k_1 a H'_n(k_1 a)}{H_n(k_1 a)} - 1\right)\beta_2\right] \\ &+ \frac{\mu'}{\mu}\left(\frac{k_1 a H'_n(k_1 a)}{H_n(k_1 a)} - \frac{k_2 a H'_n(k_2 a)}{H_n(k_2 a)}\right)\left[\left(\frac{k'_1 a J'_n(k'_1 a)}{J_n(k'_1 a)} - 1\right)\beta'_2 - \left(\frac{k'_2 a J'_n(k'_2 a)}{J_n(k'_2 a)} - 1\right)\beta'_1\right]\end{aligned} \tag{19}$$

$$\begin{aligned}\Delta_1 &= \frac{J_n(k_1 a)}{H_n(k_1 a)}\left\{\left(\frac{k'_1 a J'_n(k'_1 a)}{J_n(k'_1 a)} - \frac{k'_2 a J'_n(k'_2 a)}{J_n(k'_2 a)}\right)\left[\left(\frac{k_2 a H'_n(k_2 a)}{H_n(k_2 a)} - 1\right)\beta_1 - \left(\frac{k_1 a J'_n(k_1 a)}{J_n(k_1 a)} - 1\right)\beta_2\right]\right. \\ &+ \left.\frac{\mu'}{\mu}\left(\frac{k_1 a J'_n(k_1 a)}{J_n(k_1 a)} - \frac{k_2 a H'_n(k_2 a)}{H_n(k_2 a)}\right)\left[\left(\frac{k'_1 a J'_n(k'_1 a)}{J_n(k'_1 a)} - 1\right)\beta'_2 - \left(\frac{k'_2 a J'_n(k'_2 a)}{J_n(k'_2 a)} - 1\right)\beta'_1\right]\right\}\end{aligned} \tag{20}$$

$$\begin{aligned}\Delta_2 &= \frac{J_n(k_1 a)}{H_n(k_2 a)}\left(\frac{k'_1 a J'_n(k'_1 a)}{J_n(k'_1 a)} - \frac{k'_2 a J'_n(k'_2 a)}{J_n(k'_2 a)}\right)\left(\frac{k_1 a J'_n(k_1 a)}{J_n(k_1 a)} - \frac{k_1 a H'_n(k_1 a)}{H_n(k_1 a)}\right) \\ &\times \left\{\beta_1 - \frac{\mu'}{\mu}\left(\frac{k_1 a H'_n(k_1 a)}{H_n(k_1 a)} - \frac{k_2 a H'_n(k_2 a)}{H_n(k_2 a)}\right)\left[\left(\frac{k'_1 a J'_n(k'_1 a)}{J_n(k'_1 a)} - 1\right)\beta'_2 - \left(\frac{k'_2 a J'_n(k'_2 a)}{J_n(k'_2 a)} - 1\right)\beta'_1\right]\right\}\end{aligned} \tag{21}$$

where

$$\beta_{1,2} = \frac{1}{2}\frac{c_L^2}{c_T^2}\left(\sigma_{1,2} - (k_{1,2}a)^2\right) + n^2 - \sigma_{1,2} - 1$$

As in the previous section we plot the magnitude of the far-field scattering amplitude versus angle for steel and titanium disks in aluminum plates. Figures 3 and 4 each show three traces superimposed for different values of the dimensionless parameter γa.

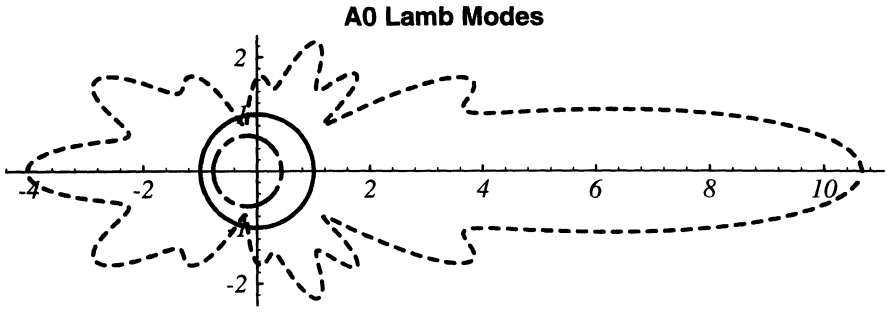

Figure 4: Angular scattering of S0-Lamb waves from in-plane titanium disk in aluminum plate. The solid line is for $\gamma a = 0.1$, the long-short dashed line is for $\gamma a = 1.0$, and the dashed line is for $\gamma a = 10$.

DISCUSSION OF RESULTS

We have derived closed-form analytic solutions for two cases of plate wave scattering from in-plane disks. The results are exact in the sense that the boundary-value problem is solved explicitly and the scattered field is written in terms of well-known functions. This allows the scattering behavior to be explored systematically both by numerical implementation of the solutions as well as by further manipulation of the explicit formulas. Special cases such as a rigid disk or a hole in a plate follow by allowing the material properties of the disk to take on limiting values.

Some comments on the applicability of these solutions for describing Lamb wave scattering from rivets need to be made, however. The most obvious deficiency in our analysis is that actual rivets are clearly not the thin disks we have assumed for our model rivets. Although our analysis does allow for the in-plane disks to have different thickness than the surrounding plate, we have assumed in formulating the problem that both the rivet and the plate are *thin*. How thin is thin enough for the relatively simple plate theories we are using to be applicable, and how much of the rivet structure needs to be accounted for, are questions that we hope to answer definitively by comparison to numerical simulations and Lamb wave experiments. Our motivation for this research is to be able to develop detailed enough models of the rivet scattering behavior so that they will be useful in developing automated algorithms for processing out disruptive rivet scattering signals from Lamb wave measurements. Numerical approaches for Lamb wave scattering are useful in understanding the scattering behavior [9] – [12], but they don't allow closed-form expressions for the scattered fields to be written down. In this work we have chosen to limit the complexity of our model by the requirement that the scattering problem be able to be solved analytically.

ACKNOWLEDGEMENTS

The author would like to thank Drs. K.J. Sun and B.T. Smith for many helpful discussions. Support for this work was provided by NASA under grant #NAG-1-1585.

REFERENCES

1. K.J. Sun and P.H. Johnston: "Effect of Rivet Rows on Propagation of Lamb Waves in Mechanically Fastened Two-Layer Aluminum Plates" in Review of Progress in Quantitative Nondestructive Evaluation, Volume 14, D.O. Thompson and D.E. Chimenti, eds. (Plenum Press, New York, (1995).
2. Y.H. Pao and C.C. Mow: "Diffraction of Elastic Waves and Dynamic Stress Concentrations" (Crane-Russak/Adam Hilger, New York/London, (1973).
3. T.R. Kane: "Reflection of Dilatational Waves at the Edge of a Plate" J. Appl. Mechanics, 79 219 (1957).
4. T.R. Kane and R.D. Mindlin: "High-Frequency Extensional Vibrations of Plates" J. Appl. Mechanics, 78 277 (1956).
5. R.D. Mindlin and M.A. Medick: "Extensional Vibrations of Elastic Plates" J. Appl. Mechanics, 80 561 (1959).
6. R.D. Mindlin: "Influence of Rotatory Inertia and Shear on Flexural Motions of Isotropic, Elastic Plates" J. Appl. Mechanics, 73 31 (1951).
7. T.R. Kane: "Reflection of Flexural Waves at the Edge of a Plate" J. Appl. Mechanics, 76 213 (1954).
8. S. Rokhlin: "Diffraction of Lamb waves by a finite crack in an elastic layer" J. Acoust. Soc. Am. 67 1157 (1980).
9. A. Safaeinili and R.A. Roberts: "An Efficient Approximate Model for Elastic Wave Scattering in Plates" in Review of Progress in Quantitative Nondestructive Evaluation, Volume 14, D.O. Thompson and D.E. Chimenti, eds. (Plenum Press, New York, (1995).
10. P. Pareige, F. Luppé and J. Ripoche: "Scattering of Lamb waves at the edge of a semi-infinite plate embedded in water" J. Acoust. Soc. Am. 92 1056 (1992).
11. G.S. Verdict, P.H. Gien and C.P. Burger: "Finite Element Study of Lamb Wave Interactions with Holes and Through Thickness Defects in Thin Metal Plates" in Review of Progress in Quantitative Nondestructive Evaluation, Volume 11, 97, D.O. Thompson and D.E. Chimenti, eds. (Plenum Press, New York, 1992).
12. S.I. Rokhlin: "Lamb wave interaction with lap-shear adhesive joints: Theory and experiment" J. Acoust. Soc. Am. 89 2758 (1991).